Buffer-gas effects on dark resonances: Theory and experiment

Michael Erhard* and Hanspeter Helm†
Department of Molecular and Optical Physics, Albert-Ludwigs-Universität, Hermann-Herder-Strasse 3, D-79104 Freiburg, Germany
(Received 20 September 2000; published 15 March 2001)

Dark resonances with widths below 30 Hz have been observed in a rubidium cell filled with neon as buffer gas at room temperature. We compare an approximate analytic solution of a Λ system to our data and show that under our experimental conditions the presence of the buffer gas reduces the power broadening of the dark resonances by two orders of magnitude. We also present numerical calculations that take into account the thermal motion and velocity-changing collisions with the buffer-gas atoms. The resulting dark-resonance features exhibit strong Dicke-type narrowing effects and thereby explain the elimination of Doppler shifts and Doppler broadening, leading to observation of a single ultranarrow dark line.

DOI: 10.1103/PhysRevA.63.043813 PACS number(s): 42.50.Gy, 32.70.Jz, 32.80.Qk

I. INTRODUCTION

Coherent population trapping has been observed in many different laser-atom systems [1]. In a three-level Λ scheme, driven by two lasers, absorption and spontaneous emission cycles create a ground-state coherence. The coherent superposition of the ground states may decouple from the laser fields by destructive interference of the absorption paths. This state does not take part in fluorescence cycles and is therefore called a dark state or dark resonance (DR). The position of the DR requires that the Raman condition be fulfilled, i.e., the difference frequency of the two lasers coincides with the energy spacing of the ground states. The absolute wavelength is of secondary importance as long as the lasers are not detuned too far off resonance. The linewidth of the DR is governed by ground-state relaxation rates and the relative phase stability of the two lasers. Despite numerous theoretical efforts to interpret the width of DRs no full understanding has yet been reached [2]. Under most experimental conditions, the ground-state relaxation is predominantly determined by the residence time of the Λ system in the laser beams [3]. The addition of a buffer gas leads to a diffusive motion of the Λ system by simultaneously preserving the ground-state coherence over millions of buffer-gas collisions [4]. Spectacularly narrow DR linewidths of 150 Hz in Rb [5] and even DRs below 50 Hz in cesium have been observed with neon as buffer gas using phase-locked diode lasers [6]. We examined DRs in spectroscopy cells on ^{85}Rb and ^{87}Rb in 6.5-kPa neon as buffer gas at room temperature and explored the effects of laser intensity and detuning on the linewidth and position of the DR. The ground-state decoherence was independently determined by the ''relaxation in the dark'' method [7].

An approximate solution of density matrix equations of motion for the simple Λ system taking into account collisional effects reveals a reduction of the power broadening of the DR. Thereby we explain the discrepancy of two orders of magnitude in previously observed and previously predicted power broadening [8]. While Doppler effects are rigorously reduced by collinear beam propagation of the two lasers, Doppler effects of the ground-state spacing frequency remain in collinear geometry. In Rb at room temperature a residual Doppler broadening of about 50 Hz is expected for the DR due to the velocity spread of contributing atoms. This width is incommensurate with the narrowest linewidths reported here. Furthermore, in a hot Doppler medium, two narrowly spaced resonances should be observed because of the presence of the two upper hyperfine-structure levels in the alkali-metal gases, which are involved in a Λ-system pair. In addition, the Doppler effect alone predicts that the DR position should move slightly, even in collinear geometry, when tuning the absolute wavelength of a laser from atomic resonance. In the presence of a low buffer-gas pressure, required to achieve the narrow linewidth to observe these effects, these effects are not observed, however. We show explicitly that velocity-changing coherence-preserving collisions (VCCPCs) in the density matrix equations of motion for a thermal distribution of a four-level system can explain the absence of these Doppler effects and the appearance of the DRs. Initially, a broadening of the DR is observed when the

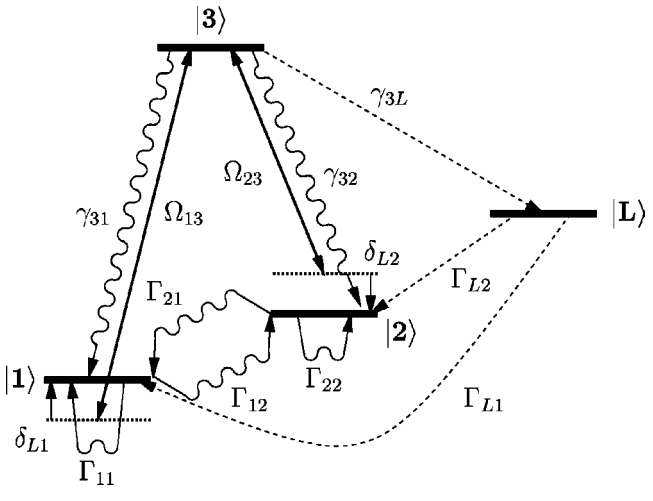

FIG. 1. Λ scheme considered depicting the ground hyperfine states (for ^{87}Rb) $|1\rangle=|^2S_{1/2},F=1,m_F=0\rangle$, $|2\rangle=|^2S_{1/2},2,0\rangle$ and the excited hyperfine state $|3\rangle=|^2P_{3/2},1,\pm1\rangle$. The reservoir of spectator states not participating in the coherent population trapping is $|L\rangle=|^2S_{1/2},\{1,2\},\neq0\rangle$.

*Electronic address: Michael.Erhard@physik.uni-freiburg.de
†Electronic address: Hanspeter.Helm@physik.uni-freiburg.de

VCCPC rate increases from zero as already reported by Graf *et al.* [9]. We show that for higher collision rates the DR experiences a Dicke-type narrowing [10] and shifts its position. This can be explained by an averaging process of the Doppler effects that is induced by frequent changes of velocities.

In Sec. II A we present the solution of a Λ-scheme model including laser fluctuations and collisional effects. In Sec. III we quantify the expected Doppler effects. A presentation of the theoretical model of the density matrix calculations taking into account thermal motion and VCCPCs and a discussion of numerical results are given in Sec. IV. Section V summarizes our experimental observations and compares the data to theory.

II. DARK RESONANCE IN A Λ SCHEME

A. Equations of motion

We consider the Λ scheme shown in Fig. 1 in the base of a rotating system defined by the transition frequencies ω_{13} and ω_{23} with the Hamiltonian

$$\hat{H}=\hbar\,\delta_{L1}|1\rangle\langle 1|-\frac{\hbar\Omega_{13}}{2}(|1\rangle\langle 3|+|3\rangle\langle 1|)+\hbar\,\delta_{L2}|2\rangle\langle 2| -\frac{\hbar\Omega_{23}}{2}(|2\rangle\langle 3|+|3\rangle\langle 2|). \tag{2.1}$$

The detunings δ_{L1} and δ_{L2} for the two lasers are defined by $\delta_{L1}=\omega_{L1}-\omega_{13}$ and $\delta_{L2}=\omega_{L2}-\omega_{23}$. In the case of ^{87}Rb, the levels $|1\rangle$, $|2\rangle$, and $|3\rangle$ refer to the $|^2S_{1/2},F=1,m_F=0\rangle$, $|^2S_{1/2},2,0\rangle$, and $|^2P_{3/2},1,\pm 1\rangle$ states, respectively [11]. A reservoir of states $|^2S_{1/2},F=\{1,2\},m_F\neq 0\rangle$ is introduced as state $|L\rangle$. The phenomenological rates γ_{ij} and Γ_{ij} are added, which stand for incoherent population transfer from state $|i\rangle$ to $|j\rangle$. The diagonal rates Γ_{ii} denote a decay rate $\Gamma_{ii}/2$ for coherences involving level $|i\rangle$. Later the coherence decay rates Δ_{ij} are introduced to discuss collisions and laser-field fluctuations.

The Liouville–von Neumann equations of motion

$$\dot{\varrho}=\frac{1}{i\hbar}[\hat{H},\varrho]-(\hat{\hat{\gamma}}+\hat{\hat{\Gamma}}+\hat{\hat{\Delta}})\cdot\varrho \tag{2.2}$$

with

$$\hat{\hat{\gamma}}+\hat{\hat{\Gamma}}+\hat{\hat{\Delta}}$$

representing the dissipation due to the γ_{ij}, Γ_{ij}, and Δ_{ij} rates read explicitly in a matrix representation

$$\dot{\vec{\varrho}}=\mathcal{M}\vec{\varrho} \tag{2.3}$$

with

$$\vec{\varrho}=(\varrho_{11},\mathrm{Re}\,\varrho_{12},\mathrm{Im}\,\varrho_{12},\mathrm{Re}\,\varrho_{13},\mathrm{Im}\,\varrho_{13},\varrho_{22},\mathrm{Re}\,\varrho_{23},\mathrm{Im}\,\varrho_{23},\varrho_{33},\varrho_{LL})^T, \tag{2.4}$$

$$\mathcal{M}=\begin{pmatrix}
-\Gamma_{12} & 0 & 0 & 0 & \Omega_{13} & \Gamma_{21} & 0 & 0 & \gamma_{31} & \Gamma_{L1}\\
0 & -D_{22} & \delta_L & 0 & \frac{\Omega_{23}}{2} & 0 & 0 & \frac{\Omega_{13}}{2} & 0 & 0\\
0 & -\delta_L & -D_{33} & -\frac{\Omega_{23}}{2} & 0 & 0 & \frac{\Omega_{13}}{2} & 0 & 0 & 0\\
0 & 0 & \frac{\Omega_{23}}{2} & -D_{44} & \delta_{L1} & 0 & 0 & 0 & 0 & 0\\
-\frac{\Omega_{13}}{2} & -\frac{\Omega_{23}}{2} & 0 & -\delta_{L1} & -D_{55} & 0 & 0 & 0 & \frac{\Omega_{13}}{2} & 0\\
\Gamma_{12} & 0 & 0 & 0 & 0 & -\Gamma_{21} & 0 & \Omega_{23} & \gamma_{32} & \Gamma_{L2}\\
0 & 0 & -\frac{\Omega_{13}}{2} & 0 & 0 & 0 & -D_{77} & \delta_{L2} & 0 & 0\\
0 & \frac{\Omega_{13}}{2} & 0 & 0 & 0 & -\frac{\Omega_{23}}{2} & -\delta_{L2} & -D_{88} & \frac{\Omega_{23}}{2} & 0\\
0 & 0 & 0 & 0 & -\Omega_{13} & 0 & 0 & -\Omega_{23} & -D_{99} & 0\\
0 & 0 & 0 & 0 & 0 & 0 & 0 & 0 & \gamma_{3L} & -D_{LL}
\end{pmatrix}, \tag{2.5}$$

where $\delta_L=\delta_{L1}-\delta_{L2}$, $D_{22}=D_{33}=(\Gamma_{11}+\Gamma_{12}+\Gamma_{21}+\Gamma_{22})/2+\Delta_{12}$, $D_{44}=D_{55}=(\gamma_{31}+\gamma_{32}+\gamma_{3L}+\Gamma_{12}+\Gamma_{11})/2+\Delta_{13}$, $D_{77}=D_{88}=(\gamma_{31}+\gamma_{32}+\gamma_{3L}+\Gamma_{21}+\Gamma_{22})/2+\Delta_{23}$, $D_{99}=\gamma_{31}+\gamma_{32}+\gamma_{3L}$, and $D_{LL}=\Gamma_{L1}+\Gamma_{L2}$. All coherences involving the level $|L\rangle$ decouple and are thus dropped.

We solve for a steady-state solution of the coherences ϱ_{13}^{∞} and ϱ_{23}^{∞} to calculate the linear susceptibilities χ_{L1} and χ_{L2}. These describe the response of the atomic dipoles to the excitation by the lasers 1 and 2. Normalized to a density of one particle per (wavelength)^3, they are

$$\chi_{L1}=\frac{3}{4\pi^2}\frac{\gamma_{31}}{\Omega_{13}}\varrho_{13}^{\infty *}, \tag{2.6}$$

$$\chi_{L2}=\frac{3}{4\pi^2}\frac{\gamma_{32}}{\Omega_{23}}\varrho_{23}^{\infty *}. \tag{2.7}$$

In the following we deal with a fixed detuning δ_{L2} for laser 2 and discuss the spectra as a function of the detuning of laser 1, δ_{L1}. For the sake of simplicity we assume equal Rabi frequencies $\Omega=\Omega_{13}=\Omega_{23}$ and decay rates $\gamma_{31}=\gamma_{32}$, $\Delta_{13}=\Delta_{23}$, and $\Gamma_{L1}=\Gamma_{L2}$. We keep on using the symbols γ_{31}, γ_{32}, Δ_{13}, and Δ_{23} to remind the reader of the origin of these rates, but equality is still postulated. Furthermore, the steady-state populations $2p_0$ of the ground states are assumed to be primarily determined by pumping rates faster than the ground-state relaxation: $\Omega,\gamma_{k1}\gg\Gamma_{ij}$. Due to symmetry the ground-state populations are equal, $\varrho_{11}^{\infty}=\varrho_{22}^{\infty}=p_0$.

For low intensities $\Omega\ll\gamma_{ij}$, Eq. (2.2) can be approximated by using constant population values $\varrho_{11}^{\infty}=\varrho_{22}^{\infty}=p_0$, $\varrho_{33}^{\infty}=0$. The approximate equations read

$$\dot{\vec{\varrho}}'=\mathcal{M}'\vec{\varrho}'+\vec{p}' \tag{2.8}$$

with

$$\vec{\varrho}=(\mathrm{Re}\,\varrho_{12},\mathrm{Im}\,\varrho_{12},\mathrm{Re}\,\varrho_{13},\mathrm{Im}\,\varrho_{13},\mathrm{Re}\,\varrho_{23},\mathrm{Im}\,\varrho_{23})^T, \tag{2.9}$$

$$\vec{p}=\left(0,0,0,-\frac{\Omega p_0}{4},0,-\frac{\Omega p_0}{4}\right)^T, \tag{2.10}$$

$$\mathcal{M}'=\begin{pmatrix} -\Gamma & \delta_L & 0 & \frac{\Omega}{2} & 0 & \frac{\Omega}{2} \\ -\delta_L & -\Gamma & -\frac{\Omega}{2} & 0 & \frac{\Omega}{2} & 0 \\ 0 & \frac{\Omega}{2} & -\gamma & \delta_{L1} & 0 & 0 \\ -\frac{\Omega}{2} & 0 & -\delta_{L1} & -\gamma & 0 & 0 \\ 0 & -\frac{\Omega}{2} & 0 & 0 & -\gamma & \delta_{L2} \\ -\frac{\Omega}{2} & 0 & 0 & 0 & -\delta_{L2} & -\gamma \end{pmatrix}, \tag{2.11}$$

and

$$\Gamma=\frac{\Gamma_{11}+\Gamma_{12}+\Gamma_{21}+\Gamma_{22}}{2}+\Delta_{12}, \tag{2.12}$$

$$\gamma=\frac{\gamma_{31}+\gamma_{32}+\gamma_{3L}}{2}+\frac{\Delta_{13}+\Delta_{23}}{2}. \tag{2.13}$$

The stationary solution can be calculated from Eq. (2.8) by setting $\dot{\vec{\varrho}}'=0$:

$$\vec{\varrho}'^{\infty}=-\mathcal{M}'^{-1}\vec{p}'. \tag{2.14}$$

As shown in Appendix A, we compare the imaginary part of χ_{L1} in the range of the DR with a Lorentzian line shape

$$\mathrm{Im}\,\chi_{L1}=\mathrm{const}-\frac{\chi_{\mathrm{DR}}(\Gamma_{\mathrm{DR}}/2)^2}{\delta_L^2+(\Gamma_{\mathrm{DR}}/2)^2}, \tag{2.15}$$

where $\delta_L=\delta_{L1}-\delta_{L2}$. The DR peak lies at the Raman resonance condition $\delta_L=0$ and the full width at half maximum Γ_{DR} of the DR is

$$\Gamma_{\mathrm{DR}}=2\Gamma+\frac{\Omega^2}{(\gamma+\delta_{L2}^2/\gamma)}+O(\Omega^4), \tag{2.16}$$

or, using Eqs. (2.12) and (2.13),

$$\Gamma_{\mathrm{DR}}\approx(\Gamma_{11}+\Gamma_{12}+\Gamma_{21}+\Gamma_{22}+2\Delta_{12})+\frac{\Omega^2}{\gamma+\delta_{L2}^2/\gamma} \tag{2.17}$$

with

$$\gamma=\frac{\gamma_{31}+\gamma_{32}+\gamma_{3L}+\Delta_{13}+\Delta_{23}}{2}. \tag{2.18}$$

The minimum width is fixed by the ground-state relaxation rate $(\Gamma_{11}+\Gamma_{12}+\Gamma_{21}+\Gamma_{22}+2\Delta_{12})$. Equation (2.17) predicts a linear increase of the width with laser intensity. The more strongly the optical transitions $1\leftrightarrow3$ and $2\leftrightarrow3$ are damped out by decay or other decoherence processes, the smaller is the power broadening of the DR.

The contrast χ_{DR} of the DR is defined as the peak height within the enveloping absorption curve [Eq. (2.15)],

$$\chi_{\mathrm{DR}}=\frac{3p_0}{16\pi^2}\frac{\Omega^2}{\Gamma\gamma}\frac{1}{(1+\delta_{L2}^2/\gamma^2)^2}. \tag{2.19}$$

The observed peak height H_{DR} (intensity signal) is proportional to $\chi_{\mathrm{DR}}I_0$ and thus proportional to the square of intensity, $H_{\mathrm{DR}}\propto I_0^2$.

B. Laser-field fluctuations

Referring to [12,13], laser fluctuations can be included by considering the additional Hamiltonian

$$\hat{H}_S=\hbar\mu_1(t)a_1^{\dagger}a_1+\hbar\mu_2(t)a_2^{\dagger}a_2. \tag{2.20}$$

The operators $a_i^\dagger$ and a_i represent creation and annihilation operators of the laser field i and the functions $\mu_i(t)$ describe frequency fluctuations. For a white-noise model the two-point correlation functions read

$$\langle \mu_i(t)\mu_j(t')\rangle = \Delta_{ij}^f \delta(t-t'), \tag{2.21}$$

where Δ_{ij}^f is a constant. By iterating the additional terms of the equations of motion

$$\dot{\varrho} + = -\frac{i}{\hbar}[\hat{H}_S, \varrho], \tag{2.22}$$

we obtain

$$\dot{\varrho}(t) + = -\frac{i}{\hbar}[\hat{H}_S(t), \varrho(0)] - \frac{1}{\hbar^2}\int_0^t dt'[\hat{H}_S(t),[\hat{H}_S(t'), \varrho(t')]]. \tag{2.23}$$

The first term can be dropped, because the time average of $\mu_i(t)$ is assumed to vanish. Expansion of the integral in Eq. (2.23) from t to ∞, which is reasonable due to the Markovian nature of the μ_i's, we end up with terms for the density matrix elements $\varrho^{n_1 n_2, m_1 m_2}$, whose superscripts n_i, m_i stand for the photon numbers in laser field i,

$$\dot{\varrho}_{kl}^{n_1 n_2, m_1 m_2} + = -[\Delta_{11}^f (n_1 - m_1)^2 + 2\Delta_{12}^f (n_1 n_2 - n_1 m_2 - n_2 m_1 + m_1 m_2) + \Delta_{22}^f (n_2 - m_2)^2] \times \varrho_{kl}^{n_1 n_2, m_1 m_2}. \tag{2.24}$$

In the semiclassical limit the levels of the Λ scheme are combined with the photon numbers

$$|1, n_1 + 1, n_2\rangle \overset{L1}{\leftrightarrow} |3, n_1, n_2\rangle \overset{L2}{\leftrightarrow} |2, n_1, n_2 + 1\rangle$$

and result in the following terms from Eq. (2.24):

$$\dot{\varrho}_{12} + = -(\Delta_{11}^f + \Delta_{22}^f - 2\Delta_{12}^f)\varrho_{12}, \tag{2.25}$$

$$\dot{\varrho}_{13} + = -\Delta_{11}^f \varrho_{13}, \tag{2.26}$$

$$\dot{\varrho}_{23} + = -\Delta_{22}^f \varrho_{23}. \tag{2.27}$$

It has been shown by solving the equations of motion for the photon fields [12,13] that Δ_{ii}^f represents the linewidth of laser i while Δ_{12}^f stands for the cross correlation of the two lasers.

Reconsidering Eq. (2.17) with the terms Δ_{ij}^f defined by Eqs. (2.25)–(2.27), the DR width reads

$$\Gamma_{\mathrm{DR}} = (\Gamma_{11} + \Gamma_{12} + \Gamma_{21} + \Gamma_{22}) + 2(\Delta_{11}^f + \Delta_{22}^f - 2\Delta_{12}^f) + \frac{\Omega^2}{\gamma + \delta_{L2}^2/\gamma} \tag{2.28}$$

with

$$\gamma = \frac{\gamma_{31} + \gamma_{32} + \gamma_{3L} + \Delta_{11}^f + \Delta_{22}^f}{2}. \tag{2.29}$$

The term $2(\Delta_{11}^f + \Delta_{22}^f - 2\Delta_{12}^f)$ stands for a DR broadening caused by laser frequency fluctuations. Observation of narrow DR linewidths therefore requires either lasers with narrow and stable line spectra or else critically cross-correlated lasers, which fulfill $\Delta_{12}^f = \frac{1}{2}(\Delta_{11}^f + \Delta_{22}^f)$. The latter is achieved by optical phase-locked diode lasers [14]. The laser linewidths Δ_{11}^f and Δ_{22}^f can be considered as additional contributions to the natural linewidths to describe the effect on power broadening of the DR width.

C. Buffer-gas collisions

The level energy shift due to a collisional process can be taken into account by an additional Hamiltonian similar to (2.20):

$$\hat{H}_S = \hbar\mu_1'(t)|1\rangle\langle 1| + \hbar\mu_2'(t)|2\rangle\langle 2| + \hbar\mu_3'(t)|3\rangle\langle 3|. \tag{2.30}$$

The functions μ_i' describe the motion in the additional potential of the Λ-system–buffer-gas atom–molecule during a collision. Assuming collisions of short duration and numerous compared to other relevant time scales it is useful to split up the functions $\mu_i' = \langle \mu_i'(t)\rangle + \mu_i(t)$ into a time-average value $\langle \mu_i'(t)\rangle$ and a fluctuating term $\mu_i(t)$ with a time-average value of zero and white-noise frequency spectrum. The time-average value can be written as

$$\Delta_i^c = \langle \mu_i'(t)\rangle = R\Delta\phi_i \tag{2.31}$$

representing an average phase of $\Delta\phi_i$ ''picked up'' per collision at a collision rate R. The contribution of the time-average value to the equations of motion is in good approximation

$$\dot{\varrho} + = -\frac{i}{\hbar}[\langle \hat{H}_S\rangle, \varrho] \tag{2.32}$$

or explicitly

$$\dot{\varrho}_{12} + = -i(\Delta_1^c - \Delta_2^c)\varrho_{12}, \tag{2.33}$$

$$\dot{\varrho}_{13} + = -i(\Delta_1^c - \Delta_3^c)\varrho_{13}, \tag{2.34}$$

$$\dot{\varrho}_{23} + = -i(\Delta_2^c - \Delta_3^c)\varrho_{23}. \tag{2.35}$$

Equation (2.33) shows up as a collisional shift $\delta^c = (\Delta_2^c - \Delta_1^c)$ of the position of the DR. The shift is proportional to the collision rate R and thus proportional to the buffer-gas pressure as observed experimentally [6].

The fluctuating part is considered in the same manner as the laser fluctuations and can be written as a contribution to the equations of motion:

$$\dot{\varrho}_{12} + = -(\Delta_{11}^c + \Delta_{22}^c - 2\Delta_{12}^c)\varrho_{12}, \tag{2.36}$$

$$\dot{\varrho}_{13}+=-(\Delta_{11}^{c}+\Delta_{33}^{c}-2\Delta_{13}^{c})\varrho_{13}, \tag{2.37}$$

$$\dot{\varrho}_{23}+=-(\Delta_{22}^{c}+\Delta_{33}^{c}-2\Delta_{23}^{c})\varrho_{23}. \tag{2.38}$$

Introducing the quantity $\Delta_{\mathrm{DR}}^{c}=2(\Delta_{11}^{c}+\Delta_{22}^{c}-2\Delta_{12}^{c})$ and assuming equal decoherence rates on the optical transitions $\Delta^{c}=(\Delta_{11}^{c}+\Delta_{33}^{c}-2\Delta_{13}^{c})=(\Delta_{22}^{c}+\Delta_{33}^{c}-2\Delta_{23}^{c})$, the DR width reads

$$\Gamma_{\mathrm{DR}}=(\Gamma_{11}+\Gamma_{12}+\Gamma_{21}+\Gamma_{22})+\Delta_{\mathrm{DR}}^{c}+\frac{\Omega^{2}}{\gamma+\delta_{L2}^{2}/\gamma} \tag{2.39}$$

with

$$\gamma=\frac{\gamma_{31}+\gamma_{32}+\gamma_{3L}+2\Delta^{c}}{2}. \tag{2.40}$$

The collisional broadening Δ_{DR}^{c} in typical alkali-metal–noble-gas collisions is very small and can be explained by highly correlated fluctuations of the potential energy in collisions of ground-state atoms with the buffer gas. We show in Appendix B that the small collisional broadening is not in contradiction to the much bigger collisional shift of the DR, $\Delta_{\mathrm{DR}}^{c}\ll|\Delta_{1}^{c}-\Delta_{2}^{c}|$. However, the optical lines are typically broadened by $2\pi\times 80\,\mathrm{kHz/Pa}$ [15], which is a result of different potential-energy curves that describe collisions for the excited- and ground-state atoms with the buffer gas. In our experiment, the inclusion of collisional broadening in Eq. (2.40) leads to a strong reduction of the power broadening of the DR as will be shown later.

D. Relaxation by diffusion

A major relaxation process appears due to spatial diffusion out of the laser beams. We define a diffusion rate Γ_{D} describing Λ systems that leave the beams. This loss is compensated by fully randomized (in the sense of a statistical classical ensemble without any coherences) Λ systems reentering the observation region. Using the general rates Γ_{ij} to describe this process within the closed system of Fig. 1, the ''diffusion probability'' of both ground states is equal, $\Gamma_{D}=\Gamma_{11}+\Gamma_{12}=\Gamma_{21}+\Gamma_{22}$. The state of the ''reentering'' system is independent of the state of the leaving system it compensates for in terms of populations: $\Gamma_{11}=\Gamma_{12}$, $\Gamma_{21}=\Gamma_{22}$. It follows that $\Gamma_{ij}=\Gamma_{D}/2$ and the contribution to the DR width is

$$\Gamma_{\mathrm{DR}}+=2\Gamma_{D}. \tag{2.41}$$

E. Total DR linewidth

As shown in Table I the total width of the DR sums up contributions due to diffusion, collisional relaxation of the ground-state coherence, phase errors between the laser fields, and a power-broadening part. The origin of power broadening can be attributed to Rabi oscillations. These are damped by optical decay, incoherent transfer to a loss channel, laser linewidths, and collisional broadening of the optical transitions (as listed in Table II). The stronger the damping the less likely that Rabi oscillations give rise to a broadening of the DR.

TABLE I. Contributions to the total DR linewidth.

Contribution		DR width
Diffusion	$\Gamma_{\mathrm{DR}}=$	$2\Gamma_{D}$
Collisional decoherence	$+$	$2\Delta_{\mathrm{DR}}^{c}$
Laser fluctuations	$+$	$2(\Delta_{11}^{f}+\Delta_{22}^{f}-2\Delta_{12}^{f})$
Power broadening	$+$	$\dfrac{\Omega^{2}}{\gamma+\delta_{L2}^{2}/\gamma}$

III. DOPPLER EFFECTS

In order to describe experiments in hot spectroscopy cells, Doppler effects caused by thermal motion of the Λ systems need to be taken into account. In the following all frequencies correspond to the rest frame of the Λ system unless they are marked by the superscript (lab), in which case they refer to the laboratory frame. Taking into account the Doppler-shifted frequencies of a Λ scheme, which moves at velocity v with respect to the beam propagation direction of the two collinear laser beams, we have

$$\omega_{L1}=\omega_{L1}^{(\mathrm{lab})}\left(1-\frac{v}{c}\right), \tag{3.1}$$

$$\omega_{L2}=\omega_{L2}^{(\mathrm{lab})}\left(1-\frac{v}{c}\right). \tag{3.2}$$

The DR condition $\omega_{L1}-\omega_{L2}=\omega_{\mathrm{hf}}$ yields a resonance frequency $\omega_{\mathrm{DR}}^{(\mathrm{lab})}$ for the DR observed in the laboratory frame of

$$\omega_{\mathrm{DR}}^{(\mathrm{lab})}=\omega_{L1}^{(\mathrm{lab})}-\omega_{L2}^{(\mathrm{lab})}=\frac{\omega_{\mathrm{hf}}}{1-v/c}\approx\omega_{\mathrm{hf}}\left(1+\frac{v}{c}\right). \tag{3.3}$$

It has been shown [16] that for our experimental parameters the main contribution to the observed DR originates from a class of atoms moving at velocity v_{i} whose Doppler effects lead to a resonance of laser i to transition $i\leftrightarrow 3$ ($\omega_{Li}=\omega_{i3}$). Taking $i=2$ and solving for v_{2} as a function of the laser 2 detuning in the laboratory frame $\delta_{L2}^{(\mathrm{lab})}=\omega_{L2}^{(\mathrm{lab})}-\omega_{23}$ results in

TABLE II. Significant contributions to the damping rate γ of the power broadening.

Contribution		Damping rate γ
Optical decay	$2\gamma=$	$\gamma_{31}+\gamma_{32}$
Optical loss channel[a]	$+$	γ_{3L}
Laser linewidths	$+$	$\Delta_{11}^{f}+\Delta_{22}^{f}$
Collisional broadening	$+$	$\Delta_{13}^{c}+\Delta_{23}^{c}$

[a]The sum of $\gamma_{31}+\gamma_{32}+\gamma_{3L}$ is equal to the spontaneous decay rate of the excited state. γ_{3L} represents the Clebsch-Gordan weighted portion of spontaneous decay into the reservoir states L.

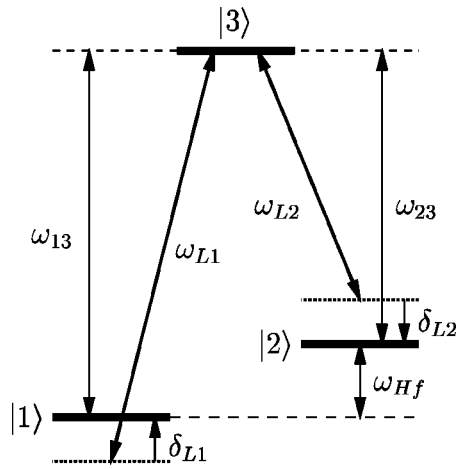

FIG. 2. Frequencies for the Λ system considered.

$$v_2 = c\,\frac{\delta_{L2}^{(\mathrm{lab})}}{\omega_{L2}^{(\mathrm{lab})}} \approx c\,\frac{\delta_{L2}^{(\mathrm{lab})}}{\omega_{\mathrm{opt}}} \tag{3.4}$$

with $\omega_{\mathrm{opt}} \approx \omega_{13} \approx \omega_{23}$, which is fulfilled in alkali-atom experiments. The position of the DR should therefore depend on the absolute laser frequency $\delta_{L2}^{(\mathrm{lab})}$ and can be expressed by

$$\omega_{\mathrm{DR}}^{(\mathrm{lab})} = \omega_{\mathrm{hf}}\left(1 + \frac{v_2}{c}\right) = \omega_{\mathrm{hf}}\left(1 + \frac{\delta_{L2}^{(\mathrm{lab})}}{\omega_{23}}\right). \tag{3.5}$$

On the other hand, the velocity spread of the contributing velocity class can be roughly determined by taking into account the optical linewidth ($2 \leftrightarrow 3$ transition) denoted by γ. The velocity spread leads to a Doppler broadening $\Gamma_{\mathrm{DR,Doppler}}^{(\mathrm{lab})}$ of the observed DR in the laboratory frame:

$$\Gamma_{\mathrm{DR,Doppler}}^{(\mathrm{lab})} = \frac{\gamma}{\omega_{\mathrm{opt}}}\,\omega_{\mathrm{hf}}. \tag{3.6}$$

In addition, the experiment uses atoms with two upper hyperfine levels spaced by $\omega_{34} \gg \gamma$ as shown in Fig. 3. In our experimental case the level $|4\rangle$ would correspond to $|^2P_{3/2}, F=2, m_F=\pm 1\rangle$ in ^{87}Rb. In the presence of the two close-lying Λ schemes, two DRs with a spacing of

$$\omega_{\mathrm{DR},3}^{(\mathrm{lab})} - \omega_{\mathrm{DR},4}^{(\mathrm{lab})} = \frac{\omega_{34}}{\omega_{\mathrm{opt}}}\,\omega_{\mathrm{hf}} \tag{3.7}$$

should be observed at finite temperature.

We have summarized typical values of these Doppler effects for our ^{85}Rb and ^{87}Rb experiments in Table III. The absence of these Doppler phenomena in buffer-gas experiments is due to velocity-changing collisions, which lead to physics completely different from the usual Doppler approach to hot gases, as we show in the following section.

TABLE III. Energy parameters for ^{85}Rb and ^{87}Rb together with the expected Doppler effects.

Parameter	^{85}Rb	^{87}Rb	Unit
$\omega_{\mathrm{opt}}/2\pi$	3.85×10^{14}	3.85×10^{14}	Hz
$\omega_{\mathrm{hf}}/2\pi$	3036	6835	MHz
$\gamma/2\pi$	6	6	MHz
$\omega_{34}/2\pi$	63	157	MHz
Doppler shift			
$\Delta\omega_{\mathrm{DR}}^{(\mathrm{lab})}/\delta_{L2}^{(\mathrm{lab})}$	7.9	17.8	Hz/MHz
Doppler broadening			
$\Gamma_{\mathrm{DR,Doppler}}^{(\mathrm{lab})}/2\pi$	47	107	Hz
DR splitting			
$(\omega_{\mathrm{DR},3}^{(\mathrm{lab})} - \omega_{\mathrm{DR},4}^{(\mathrm{lab})})/2\pi$	498	2795	Hz

IV. DARK RESONANCE IN THE PRESENCE OF BUFFER GAS COLLISIONS

A. Equations of motion

We consider a thermal distribution of the four-level system shown in Fig. 3. The incoherent loss channel represented by the level $|L\rangle$ is omitted, because it only modifies the power broadening, which is not discussed here. As in Sec. II A we consider the Hamiltonian

$$\hat{H} = \hat{H}_{\mathrm{int}} + \hat{H}_{L1} + \hat{H}_{L2}, \tag{4.1}$$

$$\hat{H}_{\mathrm{int}} = \hbar\,\delta_{L1}|1\rangle\langle 1| + \hbar\,\delta_{L2}|2\rangle\langle 2| + \hbar\,\omega_{34}|4\rangle\langle 4|, \tag{4.2}$$

$$\hat{H}_{L1} = -\frac{\hbar\Omega_{13}}{2}(|1\rangle\langle 3| + |3\rangle\langle 1|) - \frac{\hbar\Omega_{14}}{2}(|1\rangle\langle 4| + |4\rangle\langle 1|), \tag{4.3}$$

$$\hat{H}_{L2} = -\frac{\hbar\Omega_{23}}{2}(|2\rangle\langle 3| + |3\rangle\langle 2|) - \frac{\hbar\Omega_{24}}{2}(|2\rangle\langle 4| + |4\rangle\langle 2|), \tag{4.4}$$

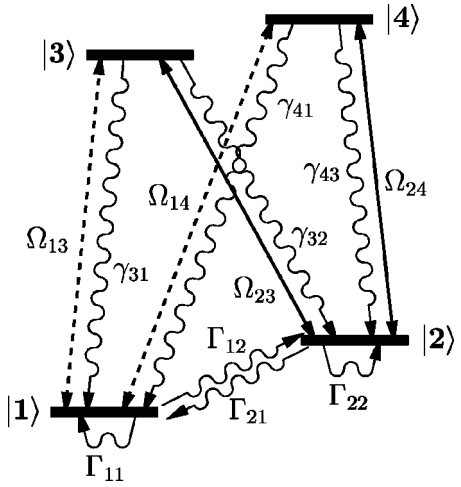

FIG. 3. Four-level system considered. State $|4\rangle$ corresponds to $|^2P_{3/2}, 2, \pm 1\rangle$ for ^{87}Rb. The other state labels are as given in Fig. 1.

and add the phenomenological rates Γ_{ij} and γ_{ij}. Applying the rotating-wave approximation, laser 1 couples to the $1\leftrightarrow3$ and $1\leftrightarrow4$ transitions and laser 2 drives the $2\leftrightarrow3$ and $2\leftrightarrow4$ transitions. The upper hyperfine-state spacing of the $3\leftrightarrow4$ levels is denoted by ω_{34}. The detunings are defined by $\delta_{L1}=\omega_{L1}-\omega_{13}$ and $\delta_{L2}=\omega_{L2}-\omega_{23}$. The equations of motion are set up in the same manner as in Sec. II and are formally represented here by

$$\dot{\vec{\varrho}}=\mathcal{M}_n\vec{\varrho}. \tag{4.5}$$

We introduce N_v velocity classes of this four-level system moving at velocities $v_1,\ldots,v_{N_v}$ in the directions parallel and antiparallel to the two collinear laser beams. The detunings $\delta_{L1,n}$ and $\delta_{L2,n}$ of Eq. (2.2) and $\mathcal{M}_n$ in Eq. (4.5) are generalized by the subscript n to refer to a specific velocity class. Due to the Doppler effect they are

$$\delta_{L1,n}=\omega_{L1}^{(\mathrm{lab})}\left(1-\frac{v_n}{c}\right)-\omega_{12}, \tag{4.6}$$

$$\delta_{L2,n}=\omega_{L2}^{(\mathrm{lab})}\left(1-\frac{v_n}{c}\right)-\omega_{23}. \tag{4.7}$$

The buffer-gas collisions are included by a collision kernel W_{nm}, $n\neq m$, describing the rate of four-level-system changing from velocity class m to n by simultaneously preserving all density matrix elements. The complete set of equations of motion therefore reads

$$\dot{\vec{\varrho}}_n=\mathcal{M}_n\vec{\varrho}_n+\sum_{m=1}^{N_v}W_{nm}\vec{\varrho}_m. \tag{4.8}$$

The diagonal elements W_{nn} represent the population losses of the velocity classes n. The demand for particle number conservation makes W_{nn} dependent on the other elements of the collision kernel. Therefore the rate out of velocity class n must coincide with the sum of rates from class n to class m with $m\neq n$,

$$W_{nn}=-\sum_{\substack{m=1\\m\neq n}}^{N_v}W_{mn}. \tag{4.9}$$

We use a one-dimensional Maxwellian velocity distribution with a most probable velocity $v_w=\sqrt{2k_BT/m}$,

$$p_n=\mathcal{N}e^{-(v_n/v_w)^2}, \tag{4.10}$$

where p_n indicates the population of velocity class n and $\mathcal{N}$ is calculated by making use of the total number of particles N,

$$\mathcal{N}=\frac{N}{\sum_{n=1}^{N_v}e^{-(v_n/v_w)^2}}. \tag{4.11}$$

The simplest collision kernel

$$W_{nm}=\frac{1}{N}\times\begin{cases}Rp_n, & n\neq m\\ R(p_n-N), & n=m\end{cases} \tag{4.12}$$

stands for completely thermalizing collisions at a collision rate R. Neglecting the dependence of the rate R on the velocity v_n is a reasonable approximation for heavy atoms in a light buffer gas for a qualitative demonstration of the effects.

The linear susceptibilities $\chi_{L1}^{(\mathrm{lab})}$ for laser 1 and $\chi_{L2}^{(\mathrm{lab})}$ for laser 2 add up contributions of all velocity classes:

$$\chi_{L1}^{(\mathrm{lab})}=\frac{3}{4\pi^2}\sum_{n=1}^{N_v}\left\{\frac{\gamma_{31}}{\Omega_{13}}\varrho_{13,n}^*+\frac{\gamma_{41}}{\Omega_{14}}\varrho_{14,n}^*\right\}, \tag{4.13}$$

$$\chi_{L2}^{(\mathrm{lab})}=\frac{3}{4\pi^2}\sum_{n=1}^{N_v}\left\{\frac{\gamma_{32}}{\Omega_{23}}\varrho_{23,n}^*+\frac{\gamma_{42}}{\Omega_{24}}\varrho_{24,n}^*\right\}. \tag{4.14}$$

B. Numerical results

The numerical results are based on the following parameters (which roughly represent our ^{87}Rb experiment): $\Omega_{13}=\Omega_{14}=\Omega_{23}=\Omega_{24}=2\pi\times15$ kHz, $\gamma_{31}=\gamma_{32}=\gamma_{41}=\gamma_{42}=2\pi\times3$ MHz, $\Gamma_{11}=\Gamma_{12}=\Gamma_{21}=\Gamma_{22}=2\pi\times32$ Hz, $\omega_{23}=2\pi\times3.85\times10^{14}$ Hz, $\omega_{12}=2\pi\times6835$ MHz, $\omega_{34}=2\pi\times157$ MHz, and $v_w=240$ m/s. The Maxwellian velocity distribution is represented by 1000 discrete velocity classes. All graphs in Figs. 4 and 5 demonstrate the dependence of the transmission spectra on the VCCPC rate. It is important to keep in mind that in real experiments the VCCPC rate is strongly related to the buffer-gas vapor pressure. For a clearer understanding of the effects related to the rate of VCCPCs we show results for constant relaxation rates and neglect the influence of the buffer-gas vapor pressure on diffusion and collisional broadening. Therefore experimental verification of the trend with the magnitude of R in Figs. 4 and 5 becomes cumbersome (e.g., a cubic observation volume of 1 m^3 would be required for the Doppler case $R=0$).

The potential-energy curves of the ground-state Ne-Rb molecule [17] allow a rough estimate of the kinetic cross section of $\sigma_k=\pi r^2\approx4\times10^{-15}$ cm^2 ($r\approx0.35$ nm). Using our experimental parameters $p=6.5$ kPa, $T=300$ K, and $\overline{v}=500$ m/s for neon, the kinetic collision rate is therefore

$$R_k=\frac{p}{k_BT}\sigma_k\overline{v}=314\ \mathrm{MHz}. \tag{4.15}$$

Assuming that the rate of completely thermalizing collisions R is smaller than the collision rate in Eq. (4.15), our experimental data should be compared to the numerical results for approximately $R=100$ MHz.

Figure 4 shows the calculated absorption of laser 1 as function of detuning $\delta_{L1}^{(\mathrm{lab})}$ for different VCCPC rates R. Here, laser 2 is resonantly tuned to the $2\leftrightarrow3$ transition of a resting four-level system, $\delta_{L2}^{(\mathrm{lab})}=0$. In each graph the DR region is expanded and shown as dashed traces. For the Doppler case, we observe three regions of increased absorption in the enveloping Doppler curve. These repumping peaks are caused by velocity classes whose $1\leftrightarrow*$ and $2\leftrightarrow*$ transitions couple resonantly to the two lasers ($*$ stands for levels 3 and

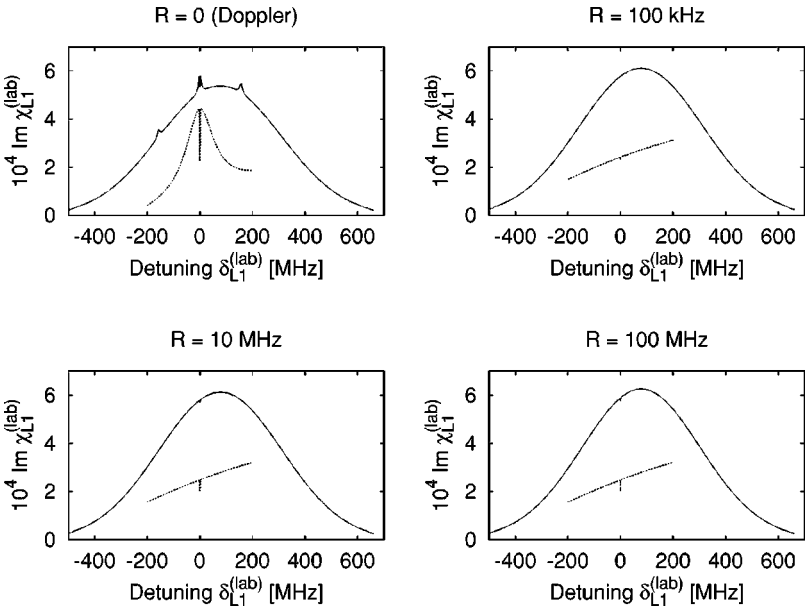

FIG. 4. Absorption (imaginary part of the linear susceptibility) of laser 1($\mathrm{Im}\,\chi_{L1}^{(\mathrm{lab})}$) as a function of the detuning $\delta_{L1}^{(\mathrm{lab})}$ for $\delta_{L2}^{(\mathrm{lab})}=0$. R denotes the collision rate of completely thermalizing collisions. The dashed traces correspond to an x axis scaled by a factor of 10 and a y axis scaled by a factor of 5 and an arbitrary y offset.

4). The ping-pong-like pumping of population between the two ground states avoids depletion of either ground-state level as occurs in other regions of the Doppler absorption curve. The association of the peaks with pumping schemes is given in Table IV. For rates $R>100\,\mathrm{kHz}>\Omega$ these peaks disappear, because the pumping process is overridden by velocity-changing and therefore resonance-changing effects (see Fig. 4).

Figure 5 illustrates the effect of VCCPCs on DRs by expanding the frequency region of interest by a factor of 10^5. In the Doppler case the DR splits up into two parts due to the two upper hyperfine-structure levels involved as already predicted in Sec. III, Eq. (3.7). For VCCPC rates of some kilohertz, the DRs are broadened. The broadening of a DR in this range of collision rates has already been demonstrated by Graf *et al.* [9]. This broadening is a result of the additional relaxation process by Λ systems leaving the resonant velocity class. However, for higher VCCPC rates, which exceed the intrinsic DR width due to relaxation ($R\gg\Gamma_R$), the DR spacing [$R\gg(\omega_{\mathrm{DR},3}^{(\mathrm{lab})}-\omega_{\mathrm{DR},4}^{(\mathrm{lab})})$], and the pumping rates [R

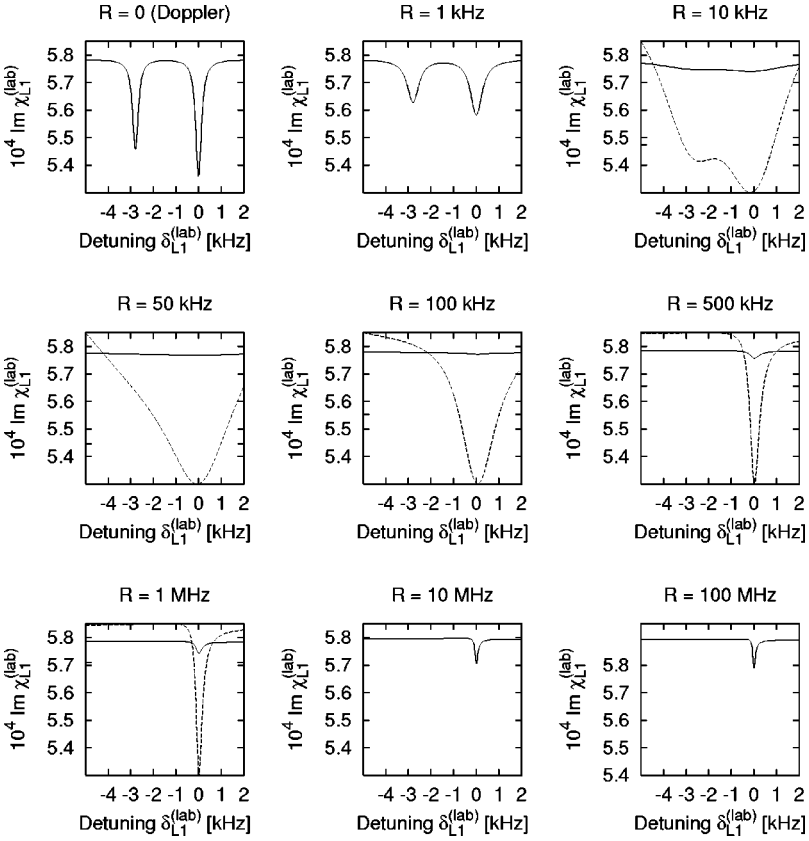

FIG. 5. Absorption (imaginary part of the linear susceptibility) of laser 1($\mathrm{Im}\,\chi_{L1}^{(\mathrm{lab})}$) as a function of the detuning $\delta_{L1}^{(\mathrm{lab})}$ for $\delta_{L2}^{(\mathrm{lab})}=0$. R denotes the collision rate of completely thermalizing collisions. The dashed lines are autoscaled and do not correspond to the y-axis label.

TABLE IV. Association of the repuming peaks of Fig. 4 with specific transitions for the Doppler case $R=0$.

$\delta_{L1}^{(\mathrm{lab})}/2\pi$ (MHz)	Laser 1	Laser 2
−157	1↔3	4↔2
0	1↔3	3↔2
	1↔4	4↔2
157	1↔4	3↔2

$\gg(\Omega^2/\gamma)$], this dissipation process surprisingly *decreases* again and the DRs merge into a single DR, with *enhanced* contrast and *narrower* than that in the pure Doppler case ($R=0$). The linewidth observed here is determined by the relaxation rates put into the numerics ($\Gamma_R=2\pi\times 128\,\mathrm{Hz}$). This can be understood when considering that all four-level systems take part in a single DR. The reason is that the large VCCPC rate makes them resonant many times during a relevant period of time. The Doppler effect is expected to be averaged over the velocity contribution $P(v)$, which leads to a DR position of

$$\overline{\delta_{L1}^{(\mathrm{lab})}}=\int dv\, P(v)\left(\omega_{\mathrm{hf}}\frac{v}{c}\right). \tag{4.16}$$

For a symmetric velocity distribution (as in our case) the Raman resonance condition $\delta_L^{(\mathrm{lab})}=\delta_{L1}^{(\mathrm{lab})}-\delta_{L2}^{(\mathrm{lab})}=0$ still applies, thus explaining the appearance of a single DR at $\delta_{L1}^{(\mathrm{lab})}=0$ ($\delta_{L2}^{(\mathrm{lab})}$ was chosen as zero for the calculations in Fig. 5). Further calculations that take into account a collisional broadening of $\Delta_{13}=\Delta_{14}=\Delta_{23}=\Delta_{24}=2.63R$ (roughly describing our experimental parameters) yield the same results as shown in Fig. 5. This is due to a collisional broadening that is smaller than the Doppler broadening in the considered range of R.

C. Dark resonances in the Dicke limit

For the sake of completeness, we demonstrate traditional Dicke narrowing [10] effects for even higher collision rates $R=1-10\,\mathrm{GHz}$ in Fig. 6 as predicted from our numerical model. The lines corresponding to the two upper hyperfine levels can be resolved at a Doppler-reduced width and a single DR is still present at $\delta_{L1}^{(\mathrm{lab})}-\delta_{L2}^{(\mathrm{lab})}=0$. For traditional

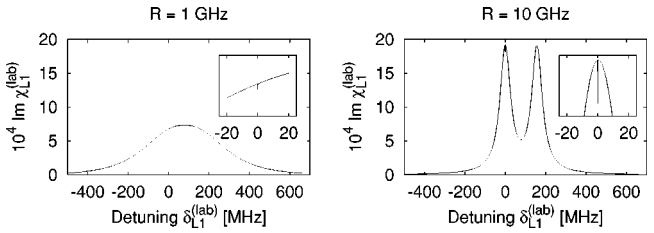

FIG. 6. Absorption (imaginary part of the linear susceptibility) of laser $1(\mathrm{Im}\,\chi_{L1}^{(\mathrm{lab})})$ as a function of the detuning $\delta_{L1}^{(\mathrm{lab})}$ for $\delta_{L2}^{(\mathrm{lab})}=0$ in the Dicke regime. R denotes the collision rate of completely thermalizing collisions. All axes of the magnified diagrams are equally scaled (note the change in frequency scale from that used in Fig. 5).

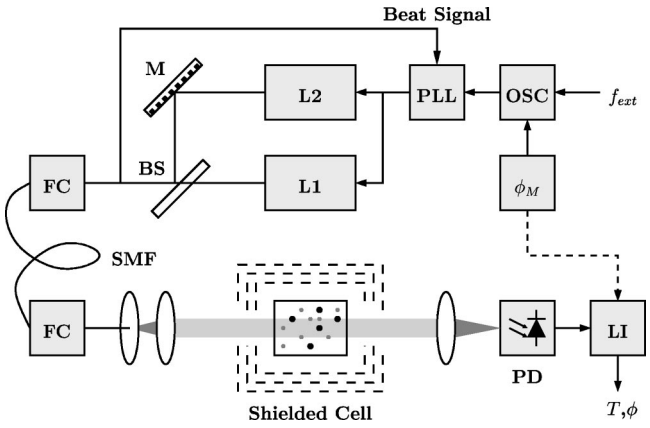

FIG. 7. Schematic of the experimental setup. Two external-cavity diode lasers ($L1$ and $L2$) are phase locked (PLL). The modulated (ϕ_M) oscillator (OSC) is externally tuned (f_{ext}) while a lock-in amplifier (L1) monitors the transmitted intensity (M, mirror; BS, beam splitter, FC, fiber coupler; SMF, single-mode fiber).

Dicke narrowing, collision rates much higher than the optical decay rates are required, $R\gg\gamma$, and the experimental realization of this regime is cumbersome at least in buffer-gas experiments.

V. EXPERIMENT

A. Setup

Our experimental setup is shown in Fig. 7. We used two external-cavity diode lasers tuned by varying temperature, cavity length, and current [18]. One laser is operated either stabilized to an atomic transition by Doppler-free saturation spectroscopy or else free running by monitoring the detuning with a Fabry-Pérot interferometer. The corresponding linewidths $\Delta\omega_{\mathrm{rms}}$ are about 60 kHz and a few megahertz, respectively. The second laser is phase locked to the first one near the frequency difference of 3036 or 6835 MHz corresponding to the hyperfine splitting of the two rubidium isotopes [19]. The achieved phase stability of about $\Delta\phi_{\mathrm{rms}}=20°$ fulfills the required critical cross correlation [the second term in Eq. (2.28) being ~ 0]. The optical phase-locked loop (PLL) is realized by superimposing both lasers on an ultrafast photodiode and mixing the electrical signal with a reference frequency of a computer-controlled microwave synthesizer to an intermediate frequency of 20 MHz. A phase-frequency detector (PD) compares the intermediate frequency signal with a 20-MHz reference source to generate two feedback signals to the cavity and current of the slave laser. Both lasers are guided through a single-mode fiber (SMF) to achieve collinearity. The beams are circularly polarized after passing the fiber, and then expanded by a telescope and passed through a room-temperature spectroscopy cell containing both rubidium isotopes and 6.5-kPa neon. The cell is magnetically shielded by three layers of μ metal. The transmission signal is refocused on a photodiode and fed into a lock-in amplifier. All DR spectra discussed here correspond to ground-state levels with $m_F=0$, a residual magnetic field of ~ 5 μT splits the DR into 11 m_F components in ^{85}Rb ($F=2,3$) and seven m_F components in ^{87}Rb ($F=1,2$). The x

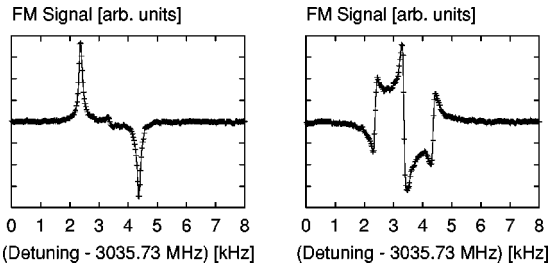

FIG. 8. DR spectra obtained by frequency-modulation spectroscopy on ^{85}Rb with $I_0=3\ \mu$W/cm^2. The left diagram shows the in-phase signal and the right diagram shows the quadrature part.

axes labeled ''detuning'' represent the frequency difference of the two lasers. The experimental radial beam profile is well fitted by the Gaussian function

$$I(r)=I_0 e^{-2(r/r_0)^2}. \tag{5.1}$$

In the experiment, the laser intensities are adjusted to be approximately equal and peak intensity I_0 and $1/e^2$ radius r_0 for one of the two lasers are specified.

A typical spectrum is shown in Fig. 8. The DR occurs on the left- and right-hand sides of the real position spaced by the modulation frequency of 1 kHz. The interested reader is refered to [20] for details on frequency-modulation spectroscopy and the interpretation of its spectra.

B. Ultranarrow linewidths

By using a $1/e^2$ beam radius of $r_0=1.44$ cm and a weak intensity of $I_0=300$ nW/cm^2 DR linewidths of 28 ± 2 Hz could be resolved as shown in Fig. 9. Repeating the measurement on consecutive days under nominally identical conditions, we obtained widths $\Gamma_{\rm DR}/2\pi=36\pm4$, 43 ± 3, 27 ± 2, and 37 ± 3 Hz. These DRs in rubidium are a factor of 5 narrower than those previously reported in rubidium [5].

We measured the frequency positions of the DRs with $m_F=0$. These values are given as $\omega_m^{(i)}$ in Table V. Comparing the value for the ^{87}Rb DR to the literature value for the hyperfine spacing [21] plus the pressure shift for 6.5-kPa neon [4], we obtain a relative deviation of -2.7×10^{-6} for our time base. This value is commensurate with the specifications of the manufacturer. Using this result to calibrate our time base, we end with a pressure shift of 1.5 ± 0.3 Hz/Pa for ^{85}Rb, with no literature value to compare to. We note that the pressure shift of the two isotopes matches the 2:1 ratio between nuclear magnetic moments in ^{87}Rb and ^{85}Rb.

TABLE V. Uncorrected measured DR positions ω_m, literature values for ω_{12} [21], and pressure shifts with neon as buffer gas.

	^{85}Rb	^{87}Rb
$\omega_m/2\pi$	3035.7334(3) MHz	6834.6837(7) MHz
$\omega_{12}/2\pi$	3035.732(1) MHz	6834.6826(1) MHz
$\delta_r/2\pi$	1.5 ± 0.3 Hz/Pa[a]	3 Hz/Pa [4]

[a]This work.

C. Linewidth and contrast as functions of intensity

We studied the width and contrast of DRs using a $2r_0=1.6$ cm diameter beam and intensities ranging from 1 to 75 μW/cm^2. The results for the width are shown in Fig. 10 and those for the height in Fig. 11. The experimental data are fitted to the formulas

$$\Gamma_{\rm DR}=\Gamma_R+\alpha I_0, \tag{5.2}$$

$$H_{\rm DR}=CI_0^n, \tag{5.3}$$

and the values obtained are presented in Table VI. In the following we compare the predictions of Eqs. (2.17), (2.28), and (2.39) with the fitted experimental results [Eq. (5.4) below]. The sum of decay rates is given by the optical decay rate $(\gamma_{31}+\gamma_{32}+\gamma_{3L})=2\pi\times6$ MHz. The collisional broadening for a neon vapor pressure of 6.5 kPa was measured by Ottinger *et al.* [15] as $\Delta_{13}^c=\Delta_{23}^c=2\pi\times263$ MHz. The coherence loss due to VCCPCs, the linewidths of the lasers, and the detuning δ_{L2} are negligible compared to the collisional broadening. The power broadening can therefore be approximated by

$$\Gamma_{\rm DR}=\Gamma_R+(2\pi)^2\times10.9\ \text{kHz MHz}\frac{\text{cm}^2}{\mu\text{W}}\times\frac{\langle I\rangle}{\Delta_{13}^c+\Delta_{23}^c}. \tag{5.4}$$

Taking into account Clebsch-Gordan coefficients of $\frac{1}{4}$ we obtain a theoretical value of $\alpha/2\pi=20.7\ \text{Hz}/(\mu\text{W cm}^{-2})$. This value is commensurate with the experimental observa-

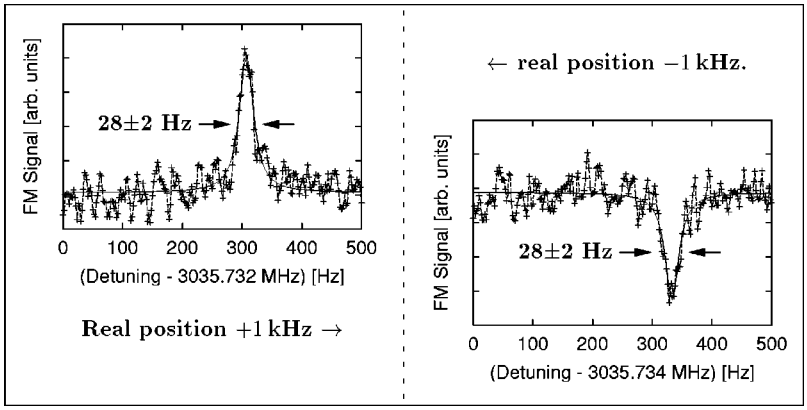

FIG. 9. Sample of the measured ultranarrow linewidths with $\Gamma_{\rm DR}/2\pi$ below 30 Hz. Parameters were $I_0=300$ nW/cm^2 and beam diameter $2r_0=2.9$ cm.

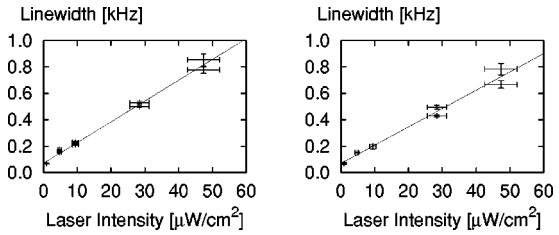

FIG. 10. Dependence of the DR width on intensity (left, ^{85}Rb; right, ^{87}Rb). The intensity values given are the peak intensities I_0 of one laser (beam diameter $2r_0=1.6$ cm).

tions in Table VI, because the latter refer to the peak intensity and do not take into account the spatial decrease of intensity over the beam profile (the observed value in Table VI being lower). We conclude that the collisional broadening is the dominant factor in power broadening and the reason for the previously noted discrepancy of two orders of magnitude from the pure Λ-system approach [22]. The asymptotic value of the DR width at zero intensity, Γ_R, will be compared to our optical pumping data in the next section. The quadratic law of the height from Sec. II A is well satisfied by the fitted values of n for Eq. (5.3) (see Table VI).

The predictions of Eq. (5.4) are also in agreement with the much narrower widths observed in the large-diameter-beam case. To demonstrate this we consider the dependence of the loss by diffusion from a cylindrical vessel of radius r_0 and length l [23],

$$\Gamma_D=\frac{D}{p}\left[\left(\frac{2.41}{r_0}\right)^2+\left(\frac{\pi}{l}\right)^2\right]. \tag{5.5}$$

The ratio of Γ_D's for the large and small diameters ($l=6.5$ cm) is $\Gamma_D(1.44\,\text{cm})/\Gamma_D(0.8\,\text{cm})=0.32$. Using the fit parameters of Table VI we predict a width for the conditions in Fig. 9 of

$$\Gamma_{\rm DR}/2\pi=0.32\times 70.3\,\text{Hz}+15.7\frac{\text{Hz}}{\mu\text{W/cm}^2}\times 0.3\frac{\mu\text{W}}{\text{cm}^2}$$
$$=27.4\pm 3.7\ \ \text{Hz} \tag{5.6}$$

in perfect agreement with the fitted linewidth in Fig. 9. Furthermore, this result confirms that diffusion is the main relaxation process in our experiments and collisional ground-state relaxation is negligible for the buffer-gas pressure used here.

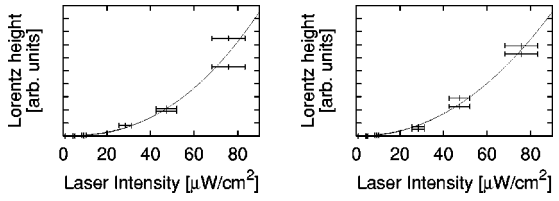

FIG. 11. Dependence of the DR height on intensity (left ^{85}Rb; right, ^{87}Rb). The intensity values given are the peak intensities I_0 of one laser (beam diameter $2r_0=1.6$ cm).

TABLE VI. Fit parameters for the dependence of the DR width and the DR contrast on intensity for ^{85}Rb and ^{87}Rb (obtained with the laser-beam diameter $2r_0=1.6$ cm at a Ne pressure of 6.5 kPa). In the last line we include the independently measured value of the ground-state hyperfine relaxation observed for the same experimental parameters (see Sec. V D).

Parameter	^{85}Rb	^{87}Rb	Unit
$\Gamma_R/2\pi$	70.3 ± 11.2	69.1 ± 27.1	Hz
$\alpha/2\pi$	15.7 ± 0.4	13.9 ± 0.9	Hz/(μW cm^{-2})
n	2.35 ± 0.32	2.12 ± 0.15	
$2\Gamma_D/2\pi$	72.8 ± 8.2	110.4 ± 37.6	Hz

D. Relaxation measurement by optical pumping

We carried out relaxation measurements using the ''relaxation in the dark'' method [4,7] with a laser-beam profile of $2r_0=1.6$ cm. A laser resonant to one transition of the Λ system depletes one lower level by optical pumping. Then the laser is interrupted and relaxation to equilibrium is allowed to take place. For different dark periods, the transmission is determined and fitted to an exponential recovery curve of absorption. The data are shown in Fig. 12. An exponential fit yields $\Gamma_D/2\pi=36.4\pm 4.1$ Hz for ^{85}Rb and 55.2 ± 18.8 Hz for ^{87}Rb. With Eq. (2.41) these independent measurements predict the relaxational contribution to the DRs to be $\Gamma_R/2\pi=2\Gamma_D/2\pi=72.8\pm 8.2$ and 110.4 ± 37.6 Hz, respectively. This independent result is in excellent agreement with the asymptotic experimental values given in Table VI.

E. DR position as a function of laser detuning

Figure 13 illustrates measurements of the DR position in ^{87}Rb for different detunings $\delta_{L2}^{(\text{lab})}$ of the fixed laser 2. The detuning range studied is up to $2\pi\times 800$ MHz. At the extreme values of detuning, Eq. (3.5) predicts that the Doppler effect should shift the DR by $2\pi\times 14.2$ kHz as indicated by the dashed trace (compare Sec. III), but no such effect is observable. Measurements of DR positions in Cs with Ne as buffer gas [24] yielded similar results, clearly demonstrating the absence of Doppler effects. The predictions of the simulations of Sec. IV that a single resonance should appear, immune to detuning $\delta_{L2}^{(\text{lab})}$, are thus confirmed experimentally.

VI. CONCLUSIONS

We have shown that, in a quantitative understanding of dark-resonance experiments in the presence of buffer gases,

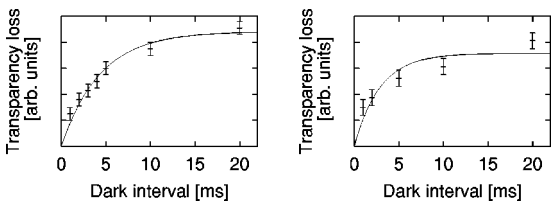

FIG. 12. Relaxation in the dark for both rubidium isotopes. Left, ^{85}Rb; right, ^{87}Rb.

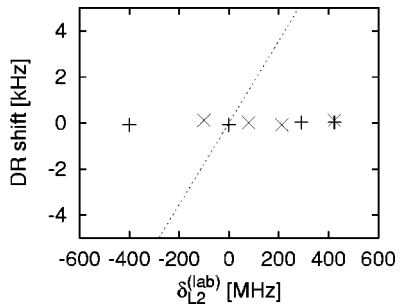

FIG. 13. Measurements of DR positions for different detunings of laser 2 for $I_0=24\,(\times)$ and 7 μW/cm^2 (+), respectively. The dashed line indicates the expected Doppler effect from Eq. (3.5) (compare Table III).

the velocity-changing process caused by buffer-gas collisions plays a major role. The power broadening in such experiments is significantly reduced due to the increased relaxation caused by the presence of buffer gas. In addition, the frequent velocity changes eliminate Doppler effects and lead to observation of spectacularly narrow lines, ultimately limited only by residence time and pressure broadening of the ground-state energy splitting. Since the latter is negligible at low alkali-metal densities [4], only a substantial and impractible increase of the observation volume could reduce DR widths below a magic 1 Hz level. In this regard the long observation time in dipole-trapped cold-atom clouds may provide a means of reaching the limit set by the currently achievable phase stability of the lasers used in preparing the dark resonance.

ACKNOWLEDGMENTS

We wish to acknowledge funding of this research by the Sonderforschungsbereich 276 (TP C16) of the German Science Foundation. Experimental support from S. Nußmann, who built the laser system, is greatly appreciated.

APPENDIX A: APPROXIMATE SOLUTION

The imaginary part of the linear susceptibility

$$\mathrm{Im}\,\chi_{L1}=-\frac{3}{4\pi^2}\frac{\gamma_{31}}{\Omega_{13}}\,\mathrm{Im}\,\varrho_{13}^{\infty} \tag{A1}$$

can be calculated from Eq. (2.14) as

$$\mathrm{Im}\,\chi_{L1}=\frac{a_0+a_1\delta_L+a_2\delta_L^2}{b_0+b_1\delta_L+b_2\delta_L^2+b_3\delta_L^3+b_4\delta_L^4} \tag{A2}$$

with

$$a_0=3\Gamma^2\gamma^2(\gamma^2+\delta_{L2}^2)+\tfrac{3}{2}\Gamma\gamma^3\Omega^2, \tag{A3}$$

$$a_1=\tfrac{3}{4}\gamma(2\gamma-\Gamma)\,\delta_{L2}\Omega^2, \tag{A4}$$

$$a_2=3\gamma^2(\gamma^2+\delta_{L2}^2)+\tfrac{3}{4}\gamma^2\Omega^2 \tag{A5}$$

and

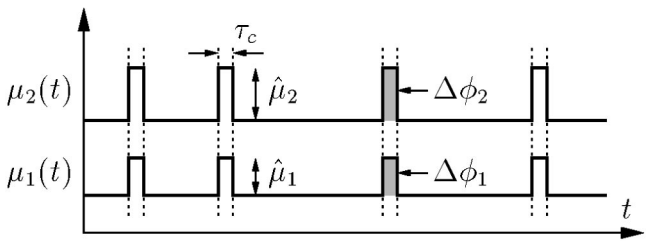

FIG. 14. Temporary evolution of the level shifts μ_i due to collisions. The shifts are assumed to be equal (average value) and of square shape with height $\hat{\mu}_i$ and collision duration τ_c. Each collision leads to an additional ''phase kick'' of $\Delta\phi_i=\hat{\mu}_i\times\tau_c$ in the coherences of level $|i\rangle$.

$$b_0=\pi^2\{16\Gamma^2(\gamma^2+\delta_{L2}^2)^2+16\Gamma\gamma(\gamma^2+\delta_{L2}^2)\Omega^2+4\gamma^2\Omega^4\}, \tag{A6}$$

$$b_1=\pi^2\{32\Gamma^2(\gamma^2+\delta_{L2}^2)\,\delta_{L2}+16\Gamma\,\delta_{L2}\Omega^2)\Omega^2\}, \tag{A7}$$

$$b_2=\pi^2\{16(\gamma^2+\delta_{L2}^2)^2+16\Gamma^2(\gamma^2+\delta_{L2}^2)+8(\Gamma\gamma+(\delta_{L2}^2-\gamma^2))\Omega^2+\Omega^4\}, \tag{A8}$$

$$b_3=\pi^2\{32(\gamma^2+\delta_{L2}^2)\,\delta_{L2}+8\,\delta_{L2}\Omega^2\}, \tag{A9}$$

$$b_4=\pi^2\{16(\gamma^2+\delta_{L2}^2)\}. \tag{A10}$$

The assumptions $\Gamma\ll\gamma$ and $\delta_L\ll\gamma$ lead to $b_3\delta_L\ll b_2$, $b_4\delta_L^2\ll b_2$, $b_1\ll b_2\delta_L$, and $a_1\ll a_2\delta_L$. Equation (A2) can then be approximated by

$$\mathrm{Im}\,\chi_{L1}\approx\frac{a_2}{b_2}\left(1-\frac{b_0/b_2-a_0/a_2}{b_0/b_2+\delta_L^2}\right). \tag{A11}$$

The full width at half maximum Γ_{DR} [compare Eq. (2.15)] is determined as

$$\Gamma_{\mathrm{DR}}\approx 2\sqrt{b_0/b_2}=2\Gamma+\frac{\Omega^2}{\gamma+\delta_{L2}^2/\gamma}+O(\Omega^4). \tag{A12}$$

In this approximation, the height of the DR χ_{DR} [compare Eq. (2.15)] reads

$$\chi_{\mathrm{DR}}\approx\frac{a_2}{b_2}-\frac{a_0}{b_0}=\frac{3}{32\pi^2}\frac{\Omega^2}{\Gamma\gamma}\frac{1}{(1+\delta_{L2}^2/\gamma^2)^2}. \tag{A13}$$

APPENDIX B: COLLISIONAL SHIFT VERSUS BROADENING

Here we show that a collisional shift of the ground-state splitting (DR) of several kilohertz (as appropriate in our experiment) is not in contradiction to the observed linewidths of 30 Hz. We assume collisions at a rate R and an average phase of $\Delta\phi_i$ ''picked up'' by level $|i\rangle$ per collision. These phases are approximated by perfectly correlated square spikes in the μ_i's of Eq. (2.30) with heights $\hat{\mu}_i$ during the collision duration τ_c (compare Fig. 14). The shift of the DR due to the considerations of Sec. II C is $\delta_c=(\Delta\phi_2-\Delta\phi_1)R$. For short collision durations the amplitudes Δ_{ij}^c of

the two-time correlation functions

$$\langle \mu_i(t)\mu_j(t')\rangle = \Delta_{ij}^c \delta(t-t') \tag{B1}$$

can by approximated by $\Delta_{ij}^c = (\hat{\mu}_i \hat{\mu}_j \tau_c)(\tau_c R)$, where the first term corresponds to the area of the convolution of the two square functions and the second term is a weighting factor due to the averaging of the correlation functions. It follows that $\Delta_{ij}^c = \Delta\phi_i \Delta\phi_j R$ and for the collisional broadening (compare Sec. II C)

$$\Delta_{\mathrm{DR}}^c = 2(\Delta_{11}^c + \Delta_{22}^c - 2\Delta_{12}^c) = 2\frac{\delta_c^2}{R}. \tag{B2}$$

For our experimental parameters of $R = 100\,\mathrm{MHz}$ and $\delta_c = 2\pi \times 9.8\,\mathrm{kHz}$, Eq. (B2) predicts $\Delta_{\mathrm{DR}}^c = 2\pi \times 12\,\mathrm{Hz}$. The observed scaling of the expected value of Γ_R (see Table VI and Sec. V C) of measurements with the small- and large-diameter laser beams suggests that the true contribution of Δ_{DR}^c to Γ_R is much smaller than this estimate. This could be explained by a collisional shift due to the wings of the long-ranging Rb-Ne potentials having smaller fluctuations than considered here.

[1] E. Arimondo, in *Progress in Optics*, edited by E. Wolf (Elsevier, Amsterdam, 1996), Vol. XXXV, Chap. V, pp. 259–354.
[2] F. Renzoni and E. Arimondo, Phys. Rev. A **58**, 4717 (1998).
[3] E. Arimondo, Phys. Rev. A **54**, 2216 (1996).
[4] W. Happer, Rev. Mod. Phys. **44**, 169 (1972).
[5] S. Brattke, U. Kallmann, and W.-D. Hartmann, Eur. Phys. J. D **3**, 159 (1998).
[6] S. Brandt, A. Nagel, R. Wynands, and D. Meschede, Phys. Rev. A **56**, R1063 (1997).
[7] A. Corney, *Atomic and Laser Spectroscopy* (Oxford University Press, Oxford, 1977).
[8] S. Nußmann, M. Erhard, M. Kemmann, and H. Helm, Verh. Dtsch. Phys. Ges. Frühjahrst. Bonn **5**, 1072 (2000).
[9] M. Graf, E. Arimondo, E. S. Fry, D. E. Nikonov, G. Padmabandu, M. O. Scully, and S.-Y. Zhu, Phys. Rev. A **51**, 4030 (1995).
[10] R. Dicke, Phys. Rev. **89**, 472 (1953).
[11] For ^{85}Rb, the F quantum numbers are increased by 1.
[12] B. Dalton and P. Knight, J. Phys. B **15**, 3997 (1982).
[13] B. Dalton and P. Knight, Opt. Commun. **42**, 411 (1982).
[14] M. Prevedelli, T. Freegarde, and T. Hänsch, Appl. Phys. B: Lasers Opt. **60**, S241 (1995).
[15] C. Ottinger, R. Scheps, G. York, and A. Gallagher, Phys. Rev. A **11**, 1815 (1975).
[16] M. Erhard, Dipl. thesis, University of Freiburg, Germany, 2000.
[17] D. Drummond and A. Gallagher, J. Chem. Phys. **60**, 3426 (1974).
[18] S. Wolf, Ph.D. thesis, University of Freiburg, Germany, 1998.
[19] S. Nußmann, Dipl. thesis, University of Freiburg, Germany, 2000.
[20] G. Bjorklund, M. Levenson, W. Lenth, and C. Ortiz, Appl. Phys. B: Photophys. Laser Chem. **32**, 145 (1983).
[21] A. Radzig and B. Smirnov, *Reference Data on Atoms, Molecules and Ions* (Springer, Berlin, 1985).
[22] E. Arimondo, in *Fundamentals of Quantum Optics III*, Vol. 420 of *Lecture Notes in Physics*, edited by F. Ehlotzky (Springer, Berlin, 1993), pp. 170–184.
[23] E. W. McDaniel and E. A. Mason, *The Mobility and Diffusion of Ions in Gases* (Wiley, New York, 1973).
[24] A. Nagel, C. Affolderbach, S. Knappe, and R. Wynands, Phys. Rev. A **61**, 012504 (1999).